

# Relict landslide detection in rainforest areas using a combination of k-means clustering algorithm and Deep-Learning semantic segmentation models

Guilherme P.B. Garcia<sup>b,d</sup>, Carlos H. Grohmann<sup>a,d,\*</sup>, Lucas Pedrosa Soares<sup>b,d</sup>, Mateus Espadoto<sup>c</sup>

<sup>a</sup>*Institute of Energy and Environment, University of São Paulo (IEE-USP), São Paulo, 05508-010, Brazil*

<sup>b</sup>*Institute of Geosciences, University of São Paulo (IGc-USP), São Paulo, 05508-080, Brazil*

<sup>c</sup>*Institute of Mathematics and Statistics, University of São Paulo (IGc-USP), São Paulo, 05508-090, Brazil*

<sup>d</sup>*Spatial Analysis and Modelling Lab (SPAMLab, IEE-USP)*

---

## Abstract

Landslides are destructive and recurrent natural disasters on steep slopes and represent a risk to lives and properties. Knowledge of relict landslides' location is vital to understand their mechanisms, update inventory maps and improve risk assessment. However, relict landslide mapping is complex in tropical regions covered with rainforest vegetation. A new CNN approach is proposed for semi-automatic detection of relict landslides, which uses a dataset generated by a k-means clustering algorithm and has a pre-training step. The weights computed in the pre-training are used to fine-tune the CNN training process. A comparison between the proposed and standard approaches is performed using CBERS-4A WPM images. Three CNNs for semantic segmentation are used (U-Net, FPN, Linknet) with two augmented datasets. A total of 42 combinations of CNNs are tested. Values of precision and recall were very similar between the combinations tested. Recall was higher than 75% for every combination, but precision values were usually smaller than 20%. False positives (FP) samples were addressed as the cause for these low precision values. Predictions of the proposed approach were more accurate and correctly detected more landslides. This work demonstrates that there are limitations for detecting relict landslides in areas covered with rainforest, mainly related to similarities between the spectral response of pastures and deforested areas with *Gleichenella sp.* ferns, commonly used as an indicator of landslide scars.

*Keywords:* landslides; deep learning; CNN; k means; CBERS-4A

---

## 1. Introduction

Landslides are destructive and recurrent natural disasters that represent a risk to lives and properties when near urban areas (Metternicht et al., 2005; Kasai et al., 2009; Netto et al., 2011; Jebur et al., 2014; Nohani et al., 2019)). They are responsible for expressive human and economic

---

\*Corresponding author

*Email addresses:* [guilherme.pereira.garcia@usp.br](mailto:guilherme.pereira.garcia@usp.br) (Guilherme P.B. Garcia), [guano@usp.br](mailto:guano@usp.br) (Carlos H. Grohmann), [lpsoares@usp.br](mailto:lpsoares@usp.br) (Lucas Pedrosa Soares), [mespadoto@gmail.com](mailto:mespadoto@gmail.com) (Mateus Espadoto)

losses worldwide, costing millions of dollars each year (Tominaga et al., 2009; Netto et al., 2011). Sendai framework for disaster risk reduction 2015-2030 (UNISDR, 2015) stated that natural hazards affected more than 25 million people and caused economic losses up to US\$ 1.3 trillion between 2008 and 2012. Landslides occur on steep slopes and are essential agents in landscape evolution by promoting changes through successive events that shape the hillsides (Wolle, 1988; Summerfield, 1991; Tominaga et al., 2009; Guzzetti et al., 2012). Deforestation, inadequate urban growth, and climate change are increasing mass movement occurrence, mainly water-related landslides such as earthflows and mudflows (Tominaga et al., 2009; Gariano and Guzzetti, 2016; Nohani et al., 2019).

Landslides have been largely studied in the last decades. Studies of landslide detection (McKean and Roering, 2004; Burns and Madin, 2009; Booth et al., 2009; Van Den Eeckhaut et al., 2011; Iwahashi et al., 2012; Guzzetti et al., 2012; Lin et al., 2013; Chen et al., 2014; Li et al., 2015; Heleno et al., 2016), susceptibility (Marcelino, 2004; Schulz, 2007; van Westen et al., 2008; Kawabata and Bandibas, 2009; Chen et al., 2013), monitoring and evaluation (Glenn et al., 2006; Du and Teng, 2007; Lingua et al., 2008; Baldo et al., 2009; Derron and Jaboyedoff, 2010; Brideau et al., 2012; Ghuffar et al., 2013; Casagli et al., 2016) are common and improve landslide risk assessment.

In recent years, ongoing technological development provided new tools for researchers which are faster, better, and more accurate than conventional ones, making data easier to gather and handle (Mantovani et al., 1996; Metternicht et al., 2005; Scaioni et al., 2014).

These new technologies significantly changed the methods of studying landslides. Conventional methods consist of extensive fieldwork, scanning of topographic maps and visual photo-interpretation of stereo images, which are costly, time consuming and have limitations that affect the quality of the data (Nilsen and Brabb, 1973; Guzzetti et al., 1999; Roering et al., 2005; Van Den Eeckhaut et al., 2005; Booth et al., 2009; Burns and Madin, 2009; Guzzetti et al., 2012; Roering et al., 2013; Scaioni et al., 2014). Use of lidar (Light Detection and Ranging) (McKean and Roering, 2004; Glenn et al., 2006; Ardizzone et al., 2007; Van Den Eeckhaut et al., 2007; Baldo et al., 2009; Burns and Madin, 2009; Kasai et al., 2009; Ventura et al., 2011; Jaboyedoff et al., 2012; Chen et al., 2013; Wang et al., 2013; Jebur et al., 2014), RPA (Remotely Piloted Aircraft) SfM-MVS (Structure from Motion Multi-view stereo) (Niethammer et al., 2010; Lucieer et al., 2014; Turner et al., 2015; Lindner et al., 2016; Yu et al., 2017; Mozas-Calvache et al., 2017; Menegoni et al., 2020; Devoto et al., 2020; Samodra et al., 2020; Xu et al., 2020; Godone et al., 2020) and process automation (Van Den Eeckhaut et al., 2007; Guzzetti et al., 2012; Van Den Eeckhaut et al., 2012; Scaioni et al., 2014; Knevels et al., 2019) are the hot spot in landslide studies which are replacing the traditional methods quickly. High resolution (HR) and very high resolution (VHR) data from both remote sensing imagery and topographic data became mandatory tools in landscape studies (Metternicht et al., 2005; Jaboyedoff et al., 2012; Scaioni et al., 2014).

Remote sensing products were under-explored in landslides studies in the 1990s and earlier decades at the expense of using aerial photographs (Mantovani et al., 1996). Satellite multi-spectral imagery and airborne photographs are generally collected after the landslide events, which makes visual identification easier due to material and vegetation removal (Guzzetti et al., 1999; Du and Teng, 2007; Booth et al., 2009; Liu et al., 2009; Burns et al., 2010; Sameen and Pradhan, 2019). Landslide mapping is vital for risk assessment studies and landslide prediction, with the generation and update of inventory maps (Sameen and Pradhan, 2019; Yu et al., 2021; Dias et al., 2021). The knowledge of the exact landslide location allows specific analysis for emergency response and precautions actions (Chen et al., 2018). In natural steep slopes, vegetation growth covers devastated areas making landslide identification harder over time when using remote sensing imagery and

difficult monitoring studies (Lehmann, 2008; Portela, 2014; Scaioni et al., 2014).

Knowledge of relict landslides is important to enhance understanding of landslide causative factors and mechanisms (Sameen and Pradhan, 2019; Li et al., 2021), to predict future events, design preventive frameworks (Schulz, 2007) and for quick landslides hazard emergency response (Chen et al., 2018). Landslide susceptibility is higher in the areas surrounding relict landslides allowing to establish a correlation between the terrain conditions of these past events and the expected ones (Schulz, 2007; Shahabi and Hashim, 2015; Zhong et al., 2019). The post-event identification from stereo photos and satellite multi-spectral imagery is commonly performed by visual interpretation of experts in GIS (Geographic Information System) software, which is an exhaustive and time-consuming task that depends on previous experience (Van Den Eeckhaut et al., 2007; Burns and Madin, 2009; Burns et al., 2010). In the last couple of decades, automatic detection of landslides started to be exploited from different sources and tools, mainly using very-high-resolution (VHR) topographic data, such as lidar DEM (Digital Elevation Model), and multispectral imagery (McKean and Roering, 2004; Glenn et al., 2006; Ardizzone et al., 2007; Van Den Eeckhaut et al., 2007; Baldo et al., 2009; Burns and Madin, 2009; Kasai et al., 2009; Ventura et al., 2011; Jaboyedoff et al., 2012; Chen et al., 2013; Wang et al., 2013; Jebur et al., 2014). OBIA (Object-based Identification Analysis) (Petropoulos et al., 2012; Van Den Eeckhaut et al., 2012; Scaioni et al., 2014; Knevels et al., 2019), pixel-based classification (Li et al., 2020; Wang et al., 2020), machine learning algorithms (Pal and Mather, 2006; Maxwell et al., 2018; Ghorbanzadeh et al., 2019; Zhong et al., 2019; Wang et al., 2020) and Deep Learning (Luus et al., 2015; Ding et al., 2016; Scott et al., 2017; Kussul et al., 2017; Chen et al., 2018; Ma et al., 2019; Sameen and Pradhan, 2019; Ji et al., 2020; Li et al., 2020; Prakash et al., 2020; Li et al., 2021; Yu et al., 2021; Soares et al., 2022) are the most prominent techniques in landslide semi-automatic and automatic detection studies. Automatic classification is important because it allows rapid mapping procedures with potential applications for hazard assessments, risk mitigation, and post-event recovery efforts (Guzzetti et al., 2012).

Machine Learning algorithms and, more recently, Deep Learning neural networks showed excellent performance in remote sensing analysis, although deep networks were not designed to process high-resolution images (Audebert et al., 2016; Cheng et al., 2017). Convolutional Neural Networks (CNN) is probably the most successful network architecture in deep learning and have been widely used to extract spatial features for object detection and semantic segmentation of high-resolution images (Krizhevsky et al., 2012; Castelluccio et al., 2015; Zhang et al., 2016; Kussul et al., 2017; Zhao et al., 2017; Cheng et al., 2018; Ma et al., 2019; Zhong et al., 2019; Li et al., 2020; Yu et al., 2021).

Studies for automatic landslide detection using CNNs are still scarce, but the results are promising, and geoscientists' interest in these techniques is increasing significantly (Ji et al., 2020). Ding et al. (2016) proposed a four-step methodology for automatic landslide detection using CNN combined with texture change detection for the Shenzhen area in China. GF-1 images were used as input in a CNN with two convolutional layers to generate feature maps used to conduct change detection using texture analysis. The proposed model achieved a recall of 100%, which means that all landslides were detected, and accuracy of 82%.

Chen et al. (2018) presented an automated approach to landslide detection using multi-temporal remote sensing imagery. The method is based on the DCNN model and the usage of STCL (Spatial-Temporal Context Learning) aiming at binary temporal NDVI (Normalized Difference Vegetation Index) and PANTEX (texture-derived built-up presence index). The proposed approach is completely automated with the detection based on the knowledge of land covering change related

to landslides without extracting samples or other manual operations. Images with different spatial resolutions were used (GF-1 (8m), Landsat 8 (30m), and Formosat-2 (8m)). Results showed that more than 70% of landslide areas were extracted.

[Sameen and Pradhan \(2019\)](#) evaluated three CNNs with different layer depths, a ResNet using different input arrangements with spectral and spatial data, and two image fusion methods for landslide detection. ResNet neural network with feature-level fusion achieved the best performance with an accuracy of 90,24%. The inputs with only spectral bands achieved the best results, and the topographic data did not improve the results for any model in this specific study.

[Ghorbanzadeh et al. \(2019\)](#) analyzed and compared current ML and CNN methods for landslide detection considering different training datasets and parameters. The training sets were constituted of spectral data (RGB + NDVI) and topographical data (Slope, Aspect, and Plan Curvature). Also, multiple input window sizes were used. The best results were achieved by CNNs based only on spectral information and 16-pixel input window size. However, CNNs did not necessarily outperform the ML methods (ANN, SVM, and RF), but only in ideal cases.

[Ji et al. \(2020\)](#) proposed a 3D attention mechanism (3D SCAM) to extract an integrated spatial-channel attention map with global consistency. The attention module was integrated into CNN structures such as VGG Net, ResNet, Inception, and Xception. The ResNet-50 boosted by the 3D SCAM achieved the best results over the other models experimented with precision, recall, accuracy, and F1-score above 95%.

[Wang et al. \(2020\)](#) proposed an integrated method that can identify relic and recent landslides from a DTM (Digital Terrain Model) using machine learning and deep learning techniques. They compared eight classification models (six machine learning algorithms and two deep learning models) and the Deep Convolutional Neural Network (DCNN) with 11 convolutional layers was the best model with accuracy as high as 92.5 %.

[Li et al. \(2021\)](#) evaluated nine of the most common deep learning models for automatic landslide detection, including VGG Net, ResNet, DenseNet, and U-Net, and used three sample sets with different sizes as input to determine both the best model accuracy and the optimal quantity of samples. All the models achieved more than 80% of accuracy. VGG Net, ResNet, and DenseNet had better performance with larger sample sets, while the performance of U-Net increased with smaller sample sets. The authors suggested that 1000 samples are optimal for deep-learning-based landslide detection if a massive amount of samples is unavailable.

[Yu et al. \(2021\)](#) proposed an end-to-end deep semantic segmentation framework of a two-branch Matrix SegNet to detect landslides from images with different spatial resolutions from four study areas. The authors adopted raw pre- and post-event images from Google Earth directly. Compared with U-Net and SegNet, the proposed Matrix SegNet showed improvements in landslide detection in F1-measure and Iou of the dataset with a spatial resolution of 2.39 m; however, the recall was smaller than 71%.

### *1.1. Objectives*

These studies show that there is no consensus on which is the best model and the best parameters for semi-automatic landslide detection. However, the results were very expressive for all the combinations of data, models, and parameters presented. This paper's main objective is to propose a new approach for semi-automatic landslide detection using CNN for an area in South-eastern Brazil and compare the results to a standard CNN approach. The focus is the detection of relict landslides partially covered by vegetation using semantic segmentation on CBERS-4A WPM

images. Detecting relict landslides may help update the inventory map of the region that is dated from the 1970s and did not suffer great reviews (Dias et al., 2021).

## 2. Methods

### 2.1. Study Area

The study area is within the Serra do Mar mountain range, southeastern Brazil (Fig. 1). It includes the majority of Caraguatatuba municipality, encompassing coastal and mountainous portions. This region is known for the preserved Atlantic rainforest and has a long history of landslides occurrences in the hillsides, mainly shallow landslides and flows (Fúlfaro et al., 1976; Guidicini and Nieble, 1984; Augusto Filho, 1992). An inventory map is available for a major event that occurred in 1967, when almost 600 landslides of various sizes were identified, which caused destruction and human losses (Fúlfaro et al., 1976). Despite the high landslide occurrence rate in the region, there is a lack of landslide documentation, with few studies updating the previously inventory map and monitoring the landslides (Correa et al., 2017; Dias et al., 2021).

A mountainous landscape marks the study area in the west and the coastal areas with sand beaches and plains in the east (Ponçano, 1981) (Fig. 2A). The mountains are characterized as rugged relief with high slope gradients and valleys with amplitudes higher than 100 m, defined as Costeira Province (Almeida, 1964; Ponçano, 1981). The landslides usually occur in this section due to its favorable conditions for mass movements.

The geological setting is within the Mantiqueira Province, specifically in Serra do Mar Domain (Perrota et al., 2005), mainly composed of granites and gneisses from the Costeiro Complex and Pico do Papagaio Complex, which occurs as intercalated lenses controlled by shear zones (Fig. 2B). Several faults and shear zones oriented towards SW-NE comprising the structural framework of the study area (Perrota et al., 2005). The principal structure is the shear zone that occurs in the N-NW portion of the study area, namely the Bairro Alto Shear zone; other important structures are the Caraguatatuba fault and the Camburu fault. These structures control lithology. There is also the presence of mafic intrusions related to the Araçuaí - Rio Doce orogen, quaternary deposits occur in river banks and coastal plans.

The local climate also contributes to landslide occurrence with rainy summers that usually trigger landslides and other mass movements (Conti and Furlan, 1996). Caraguatatuba climate is defined as Cwa, or altitude tropical climate, by Koeppen (1948). The annual average rainfall is up to 1830 mm, with August as the driest month (60 mm) and January as the rainiest (300 mm).

Most of the study area is within the Atlantic rainforest biome, which covers almost all Brazilian coastal parts and presents great biodiversity. The Dense Ombrofile Forest is the predominant vegetation cover, distinguished by high indices of temperature and rainfall during the year (Ellenberg and Mueller Dombois, 1967; Veloso et al., 1991). Marked by evergreen vegetation cover with several layers, a canopy that can reach up to 50 m in height, and dense shrubbery detaching ferns, bromeliads, and palm trees (Portela, 2014). Forest formation is controlled by elevation due to its mountainous context and can be divided into Dense Ombrofile Forest, Arboreal Forest, and Secondary vegetation (Kronka et al., 2007).

Despite the preserved vegetation in most of the study area, the landslides occur on natural steep slopes but are more common in deforested areas and close to roads and urban areas.

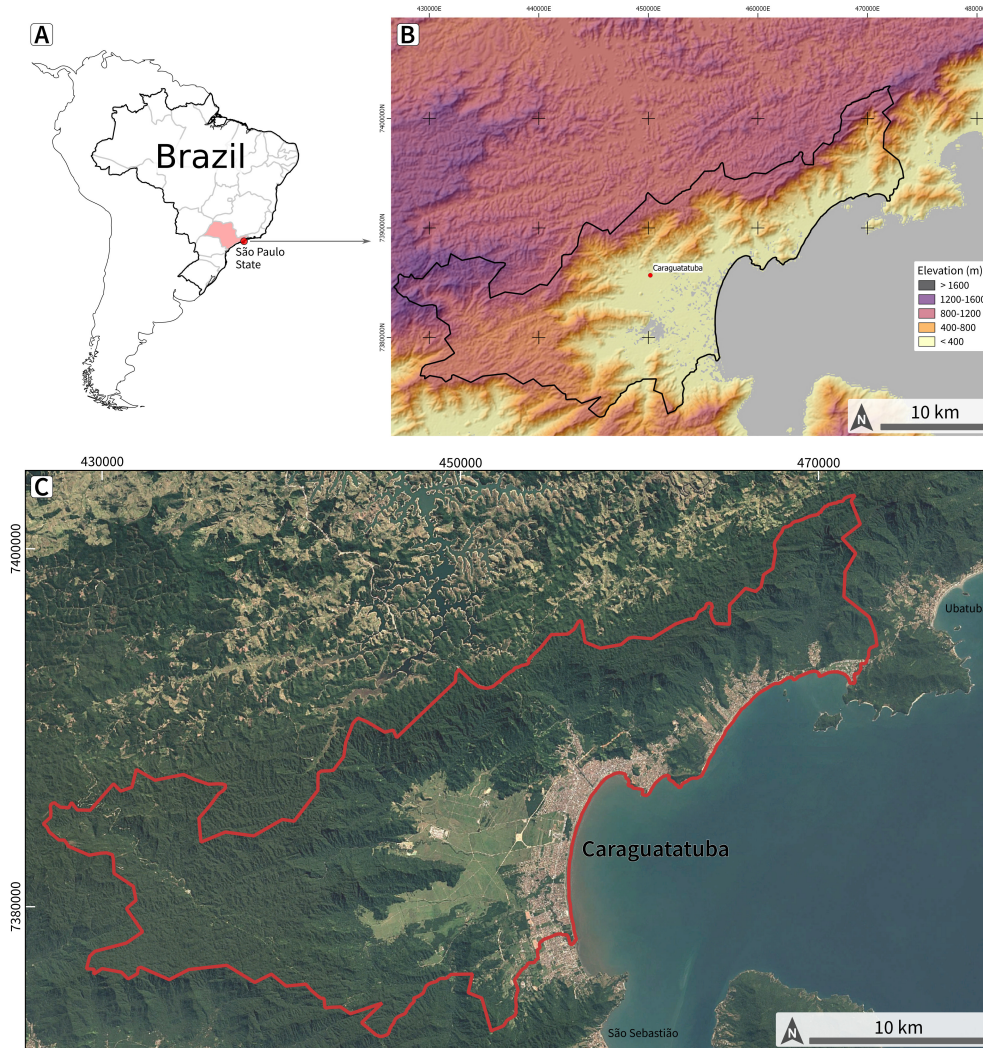


Figure 1: A) Location of São Paulo state in Brazil. B) Elevation map of the study area. C) Image of the study area with Caraguatatuba municipality in red. Satellite image Landsat/Copernicus (2015-12-30), powered by Google. UTM coordinates, zone 23 (South), WGS84.

### 2.1.1. *Gleichenella sp.*

Ferns are common plants in the Atlantic rainforest of Serra do Mar being pioneers and efficient in regenerating degraded forest (Lehmann, 2008). The hillsides degraded by landslides in the study area are usually covered by a specific fern species named *Gleichenella sp.* while others are almost totally recovered by the forest (Lehmann, 2008; Portela, 2014) (Fig. 3). *Gleichenella sp.* usually prevents complete forest regeneration in the degraded areas, maintaining the landslide scar and boundaries distinguishable from adjacent areas.

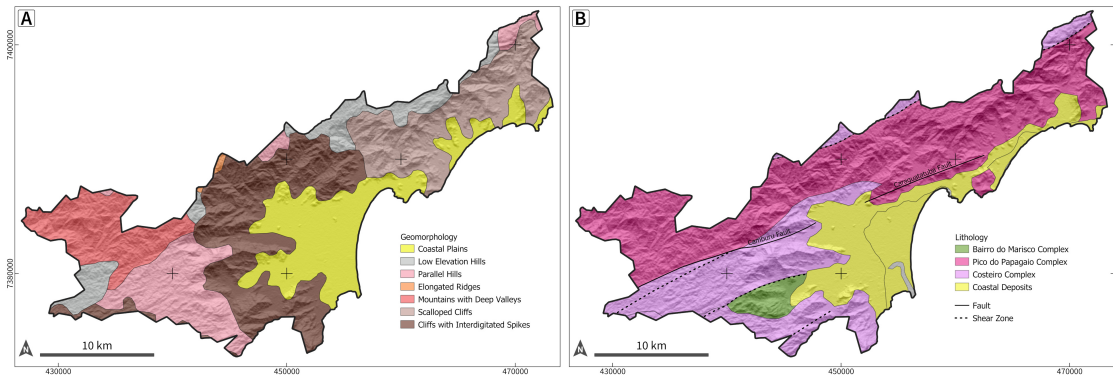


Figure 2: A) Geomorphological and (B) geological map of the study area. UTM coordinates, zone 23 (South), WGS84.



Figure 3: Example of *Gleichenella* ferns occurrence in landslide scars in Caraguatatuba municipality. Satellite imagery ©2021 Digital Globe, powered by Google. See location in Figure 1

## 2.2. Data

### 2.2.1. CBERS-4A

CBERS-4A is a mid-resolution remote sensing satellite in a sun-synchronous orbit launched in December 2019, with the first images released for download in January 2020. The satellite is operated by the Brazilian National Institute of Spatial Research (INPE) and the images are available for free download on their website (<http://www2.dgi.inpe.br/catalogo/explore>). It is equipped with three cameras: MUX (Multispectral Camera), WFI (Wide Field Imager), and WPM (Wide Panchromatic Multispectral). MUX and WFI have four optical bands (R, G, B, and NIR) with spatial resolution of 16.5 m and 55.5 m, respectively. WPM has five bands (R, G, B, NIR, and Panchromatic) with spatial resolution of 8 m for the optical bands and 2 m for the panchromatic. The revisit period is 31 days for the WPM and MUX and five days for the WFI. The swath width for each camera is 92 km (WPM), 95 km (MUX), and 684 km (WFI).

In this project were used five CBERS-4A images with the four optical bands of the WPM camera namely blue (0,45 - 0,52  $\mu\text{m}$ ), green (0,52 - 0,59  $\mu\text{m}$ ), red (0,63 - 0,69  $\mu\text{m}$ ) and near-infrared (0,77 - 0,89  $\mu\text{m}$ ). All the images were used without radiometric or atmospheric corrections and with no cloud cover.

### 2.3. Convolutional Neural Networks

CNN has shown impressive performance in many applications, including remote sensing analysis, with fast growth in the use of this network in the last few years (Krizhevsky et al., 2012; Castelluccio et al., 2015; Cheng et al., 2018). It has evolved from multilayer perceptron (MLP) (Werbos, 1974), being the first CNN proposed by Fukushima (1980) and later refined by LeCun et al. (1989) that proposed the LeNet-5. The typical architecture of a CNN is composed of multiple feature-extraction stages where each stage consists of a series of layers, including convolutional layers, pooling layers, and fully connected layers (Castelluccio et al., 2015; Cheng et al., 2018). CNN is designed to take advantage of the two-dimensional structure of the input image and focus on bridging the low-level features to high-level semantics of the image scene, automatically extracting intrinsic features from remote sensing imagery (Zhang et al., 2016; Zhong et al., 2017). For Zhao et al. (2015) a limitation for using CNN in remote sensing image classification is that it requires many labeled training samples for training the network, which is not always available.

There are many different CNNs, each with pros and cons, developed for specific tasks like classification or semantic segmentation. Some well known models are the ALEXNet (Krizhevsky et al., 2012), VGG (Simonyan and Zisserman, 2014), CaffeNet (Jia et al., 2014), GoogleNet (Szegedy et al., 2015), U-Net (Ronneberger et al., 2015), ResNet (He et al., 2016) and Densenet (Huang et al., 2017). So it is up to the researcher to evaluate and choose the best model to fit its study. In this study, three of the four available CNNs in the segmentation models python library (Yakubovskiy, 2019) were used to train the data and compare the results. The CNNs used were U-Net (Ronneberger et al., 2015), FPN (Lin et al., 2017) and Linknet (Chaurasia and Culurciello, 2017) (Fig. 4). These CNNs are built explicitly for semantic segmentation tasks rather than classification.

DenseNet (Huang et al., 2017) was used as a backbone for a pre-training step and was proposed as a network with a different connectivity pattern that connects each layer to every other layer in a feed-forward fashion, namely Dense Convolutional Network (DenseNet) (Fig. 4). A remarkable difference between DenseNet and other networks, such as ResNet, is that it yields condensed models by feature reuse that are easy to train and more efficient. It also concatenates feature maps learned by different layers, which increases variation and efficiency. The DenseNet architecture comprises dense blocks and transition layers, with a convolution at the beginning and a softmax classifier at the end.

#### 2.3.1. Deep Learning Architectures for Image Segmentation

The U-Net architecture was introduced by Ronneberger et al. (2015), modifying and extending FCN (Fully Convolutional Network) by working with very few training images, with more accurate segmentation and preserving image localization. The main difference from traditional CNN lies in its architecture of the expanding path. U-Net consists of two paths: a constructive path and an expansive path (Fig. 4). The constructive path follows the typical CNN architecture with convolution and pooling layers for downsampling. The expansive path consists of upsampling the feature map and replacing the fully connected layers.

Feature pyramids are a primary component in recognition systems for detecting objects at different scales. The Feature Pyramid Network (FPN) was introduced by Lin et al. (2017) as

a feature pyramid with rich semantics at all levels, is built quickly from a single input image scale, and is a generic solution built inside a deep ConvNet. Their architecture combines low-resolution, semantically strong features, with high-resolution, semantically weak features, by a top-down pathway and lateral connections (Fig. 4). The pyramid’s construction involves two parts: a bottom-up pathway and a top-down pathway, and the lateral connections between them.

LinkNet is a neural network architecture proposed by [Chaurasia and Culurciello \(2017\)](#) designed specifically for semantic segmentation (Fig. 4). It comprises an encoder-decoder pair containing residual blocks and linking each encoder with a decoder to avoid losing spatial information. The input of each encoder layer is bypassed by the output of its corresponding decoder so that the decoder and the upsampling operations can use the spatial information. LinkNet results were more efficient compared to existing state-of-the-art segmentation networks that have an order of magnitude larger computational and memory requirements.

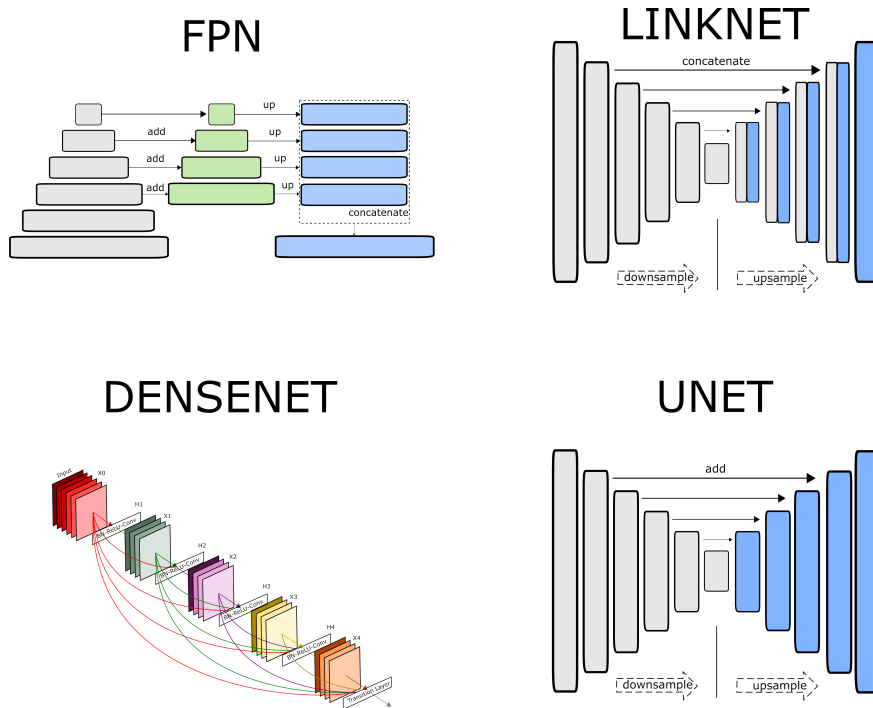


Figure 4: Structure of FPN, LINKNET and U-Net. Modified from [Yakubovskiy \(2019\)](#)

### 2.3.2. Proposed Deep Learning Approach

This study proposes a new deep learning approach for semi-automatic landslide detection, and the results are compared to a standard CNN approach. The standard approach is usually performed in three steps: data processing, training, and validation, while the proposed approach has one more step, pretraining.

- Data Processing

Two datasets were created in the data processing step, the Labeled dataset (LD) and the Cluster Dataset (CD). The Labeled Dataset (LD) comprises images labeled in two classes,

with or without landslide scars. It uses the CBERS-4A path 201 row 143 image from August of 2020 as input with a dimension of 14210 x 14592 pixels was clipped in tiles of 32 x 32 pixels. A zero-padding process was used to enable the creation of the tiles. Each tile received a label due the existence of landslide (label = 1) or not (label = 0). The landslide scars used in this labeling process were acquired from [Fúlfaro et al. \(1976\)](#) inventory map and visual interpretation of current images.

The Cluster dataset (CD) used the k-means algorithm to cluster data by trying to automatically separate samples into  $k$  groups based on similarity ([Pedregosa et al., 2011](#)). This method segments the image based on pixel color similarity, which may be able to segregate major land cover areas such as vegetation cover and urban areas. An area larger than the study area was used as input. Images covering the full extension of the Serra do Mar mountain range were used in this step, almost encompassing the whole coast of São Paulo state. Five CBERS-4A images were used as input (path/row): 200/142, 200/143, 201/142, 201/143 and 202/143. The images were clipped in tiles with 32 x 32 pixels, also using the zero-padding process for the borders of the images. Each tile receives a label with the predominant class according to the k-means clustering results. The number of clusters has to be specified for the k-means algorithm. In this study, the clustering was performed with values 2, 4, 6, 8, 10, and 12. To enhance the clustering process, pixels representing ocean and urban coastal areas were removed from input images, so the k-means algorithm used only highland and mountain features. Lastly, a class balancing process was performed with the tiles assigned to each cluster.

The study area was split into train and test areas. The test area is a minor region with few landslide scars that will be used to evaluate the accuracy of the CNNs. It was clipped from the original image and did not participate in the training process (Fig. 5).

- Pre Training

Densenet121 was chosen for this pre-training step, and the input was the Cluster dataset (CD), which was explicitly created to pre-train the backbone network. Densenet121 neural network is available as the standard backbone in the segmentation models python library ([Yakubovskiy, 2019](#)). The pre-training step intends to initialize the CNN, i.e., enable the CNN to learn how to segregate objects through the image bands automatically. As spectral features of landslides are usually different from adjacent areas, the pre-training step may help to detach these areas. The weights computed in this process will be used in the proposed approach to fine-tune the training process of the CNNs.

- Augmentation

Usually, a massive amount of data is necessary for training a neural network such as CNN, which is not always available for the researchers ([Zhao et al., 2015](#)). To overcome this lack of training samples, researchers can use data augmentation techniques to increase the number of training samples ([Ronneberger et al., 2015](#)). This study performed three types of data augmentation techniques: horizontal flip, vertical flip, and a combination of both (horizontal-vertical flip). To avoid unbalancing data, the augmentation was performed only for the positive class of the Labeled Dataset (LD). In total 365 tiles were labeled as landslide which were augmented by a factor of 30 (10950 tiles) and 50 (18250 tiles); this augmented

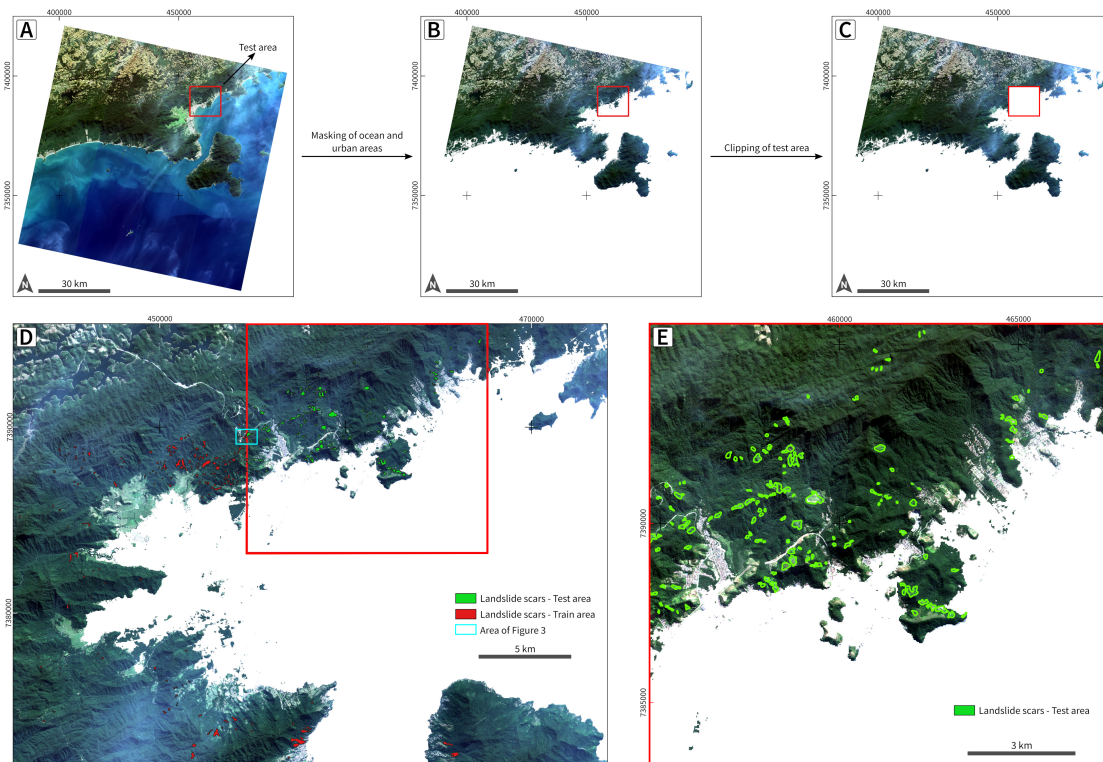


Figure 5: A) CBERS-4A image 201/143 with the location of the test area. B) Image with ocean and urban areas clipped. C) Image with the test area clipped, used for the training process. D) Landslide scars in the train area and test area. E) Test area with landslide scars.

dataset is referred to as LD30 and LD50, respectively. These augmented datasets were used in the training process for both the standard and the proposed CNN approach.

- Training

Three CNNs were used for landslide detection: FPN, Linknet, and U-Net. These CNNs are available in the Segmentation Models python library based on Keras(Tensorflow) (Yakubovskiy, 2019) and are specific for semantic segmentation tasks. All three CNN models have a down-sample and an upsample path and use the Densenet121 as a backbone. The weights from these CNNs are evaluated in the test area by validation indices and prediction of landslides. The standard approach used both LD30 and LD50 as input to train each CNN and compute the weights for later validation. A total of 6 combinations were made, and the results were used to predict landslides. In the proposed approach, the weights learned in the pre-training step were used to fine-tune the training process. The CNNs were trained for every cluster with LD30 and LD50 as input, resulting in 12 combinations for each CNN (FPN, Linknet, U-Net), 36 in total, used for model evaluation.

- Accuracy Assessment

Precision and Recall were used to validate the models. These statistical methods are based on three kinds of classified pixels: True Positives (TP), False Positive (FP), and False Negative

(FN) (Ghorbanzadeh et al., 2019). Precision is used to quantify the rate of positive samples (TP) among predicted positive samples (TP + FP). The higher the precision of the model, the better the probability of correctly classifying positive samples. In other words, precision determines how many of the classified areas are really landslides. Recall represents the ratio of correctly predicted landslides to the ground truth (Ji et al., 2020). It means that recall can determine how much of the landslide areas defined by visual interpretation were classified in the images (Ghorbanzadeh et al., 2019).

Evaluation Index	Equation
Precision	$\frac{TP}{TP+FP}$
Recall	$\frac{TP}{TP+FN}$

Table 1: Math expression of the evaluation indices. Where TP refers to True Positive, FP to False Positive and FN to False Negative

### 3. Results and Discussion

**Validation Indices** The results were evaluated by Precision and Recall validation indices and by landslide predictions that enable visual interpretation. All the combinations of CNNs and parameters were trained and validated in the train area, while the results were obtained from the test area. Tables 2 and 3 show the values of precision and recall for every combination tested.

The results are very similar between the standard CNN approach and the proposed approach and within the combinations. Recall was higher than 75% for every combination tested. The best result for the standard approach was 79.53% (U-Net with LD30) and 81.09% (Linknet with 4 clusters and LD50) for the proposed approach.

In contrast with Recall results, Precision values were usually between 10% and 20%. The higher values of precision were 15.83% for U-Net with LD50 in the standard approach and 20.47% of FPN with 8 clusters and LD30 for the proposed approach. These low precision values may indicate that the models have a high false positive rate (non-landslide pixels classified as landslides).

Recall and precision results for landslide detection are commonly above 70% (Chen et al., 2018; Ding et al., 2016; Ghorbanzadeh et al., 2019; Ji et al., 2020; Li et al., 2021; Wang et al., 2020; Yu et al., 2021; Zhong et al., 2019). Nonetheless, maximizing both evaluation indices may be challenging as they present an inverse correlation, i.e., increases in recall often come at the expense of decreases in precision. These results mean that the CNNs tested in this study predicted more landslides than existed in the ground truth, which generated a large number of False Positives that decreased precision values.

Landslide detection studies aim to create tools to perform automatic landslide detection in replacement to conventional methods such as expert visual interpretation. These studies are valuable in updating inventory maps after landslide occurrences when new landslides are identified. So it is interesting that these methods for automatic landslide detection can predict more landslides than the ones in the ground truth used for validation. In other words, False Positive samples may indicate new landslide occurrences in the study area. Therefore it is suitable for landslide detection studies to have less conservative models with higher recall and lower precision values.

Number of clusters	Dataset	FPN	U-Net	Linknet
2	LD30	0.1144	0.1270	0.1367
4	LD30	0.1755	0.0537	0.1902
6	LD30	0.1425	0.1875	0.1779
8	LD30	0.2047	0.1644	0.0555
10	LD30	0.0687	0.1655	0.1732
12	LD30	0.1328	0.1676	0.1674
2	LD50	0.0473	0.1431	0.1366
4	LD50	0.0876	0.0621	0.1752
6	LD50	0.1542	0.1585	0.1546
8	LD50	0.1836	0.1428	0.0612
10	LD50	0.1786	0.0627	0.0471
12	LD50	0.1323	0.1723	0.1613

Table 2: Precision results of FPN, U-Net and Linknet models tested for the proposed approach.

Number of clusters	Dataset	FPN	U-Net	Linknet
2	LD30	0.7618	0.7824	0.7749
4	LD30	0.7669	0.7965	0.7828
6	LD30	0.7820	0.7914	0.7866
8	LD30	0.7710	0.7944	0.7795
10	LD30	0.7602	0.7956	0.8056
12	LD30	0.7696	0.7775	0.7815
2	LD50	0.7581	0.7782	0.7828
4	LD50	0.7788	0.7886	0.8109
6	LD50	0.7765	0.7798	0.7832
8	LD50	0.7750	0.7800	0.7996
10	LD50	0.7853	0.8095	0.7906
12	LD50	0.7692	0.7877	0.7970

Table 3: Recall results of FPN, U-Net and Linknet models tested for the proposed approach.

Dataset	FPN	U-Net	Linknet
LD30	0.1337	0.1405	0.1212
LD50	0.1264	0.1583	0.1240

Table 4: Precision results of the standard approach.

Dataset	FPN	U-Net	Linknet
LD30	0.7845	0.7952	0.7774
LD50	0.7750	0.7925	0.7892

Table 5: Recall results of the standard approach.

## Predictions

The prediction maps of landslides enable visually evaluating the CNNs ability to detect landslides. Predictions were very heterogeneous among all tested combinations, and many could not classify any landslide in the area. Others were very noisy and with errors. However, some predic-

tions correctly classified most of the landslide scars but not without errors and misclassification, mainly false positives. All the predictions were performed with a threshold of 0.5.

Although recall assessment showed high results for all the combinations from both approaches, mainly above 75%, predictions showed that only 18 of 42 (36 + 6) combinations were able to identify the landslide scars more or less accurately (Fig. 6). Most of the predictions did not identify any landslide scars or had a coarse aspect with many False Positives. The supplementary material presents all 18 predictions that correctly identified landslides with TP, FP and FN results.

The predictions of the proposed approach were better than those of the standard approach. 15 of 36 (41.7%) predictions of the proposed approach identified landslide scars in the test area but always with the presence of false positives. Figure 7 shows predictions of the CNNs with 8 clusters and LD50, as well as TP, FP and FN results.

In general, these predictions managed to delineate the landslide scars mainly located in the center-north portion of the test area. Predictions of U-Net (6 clusters and LD50) and Linknet (6 clusters with LD30 and LD50) identified only the landslide scars in the center-south portion (Fig. 6).

It is not clear why this difference in classification between area portions occurs. The southern portion of the study area represents mainly urban, and ocean areas that were removed from the original image in the data processing step, and the voids were labeled as 'no data.' The image tiles used as input for the CNN were generated from this clipped image, so the 'no data' values may have affected CNN landslide detection accuracy. That may explain why the landslides in the southern portion were more complex to detect than those from the center-north portion of the study area.

For the standard approach, only 3 of 6 (50%) predictions (Linknet with LD30/LD50 and U-Net with LD30) correctly identified landslide scars, but the latter also showed a lot of false positives and had a noisy representation similar to salt-and-pepper effect. However, despite being less accurate than the proposed approach predictions, these predictions were able to identify the landslide scars from every portion of the test area, the center-north, and the center-south.

### **Correlation**

The attempt to determine an optimal combination of parameters was unsuccessful. Recall and precision values of the proposed approach showed high similarities for every combination, while the predictions were very diverse. It was not possible to establish a correlation between the parameters used and the accuracy of the results. The same happened to the standard approach.

U-Net neural network is commonly used for semantic segmentation in other studies of landslide detection (Prakash et al., 2020; Li et al., 2021; Soares et al., 2022), so it was expected to yield better results than FPN and Linknet. Although U-Net yielded the best results for recall and precision, the difference to FPN and Linknet results was not so relevant, never greater than 5%. The same happened with the predictions of landslides, where U-Net results were not superior to FPN and Linknet. U-Net and Linknet predictions have similarities with landslides predicted in the same regions, most in the center-north portion of the test area, and many false positives samples. FPN predictions were very different from U-Net and Linknet, with few false positive samples but many false negative.

It was not possible to establish an optimal combination of parameters for landslide detection, but combinations with 4 and 8 clusters yielded the best predictions for all CNNs with both LD30 and LD50.

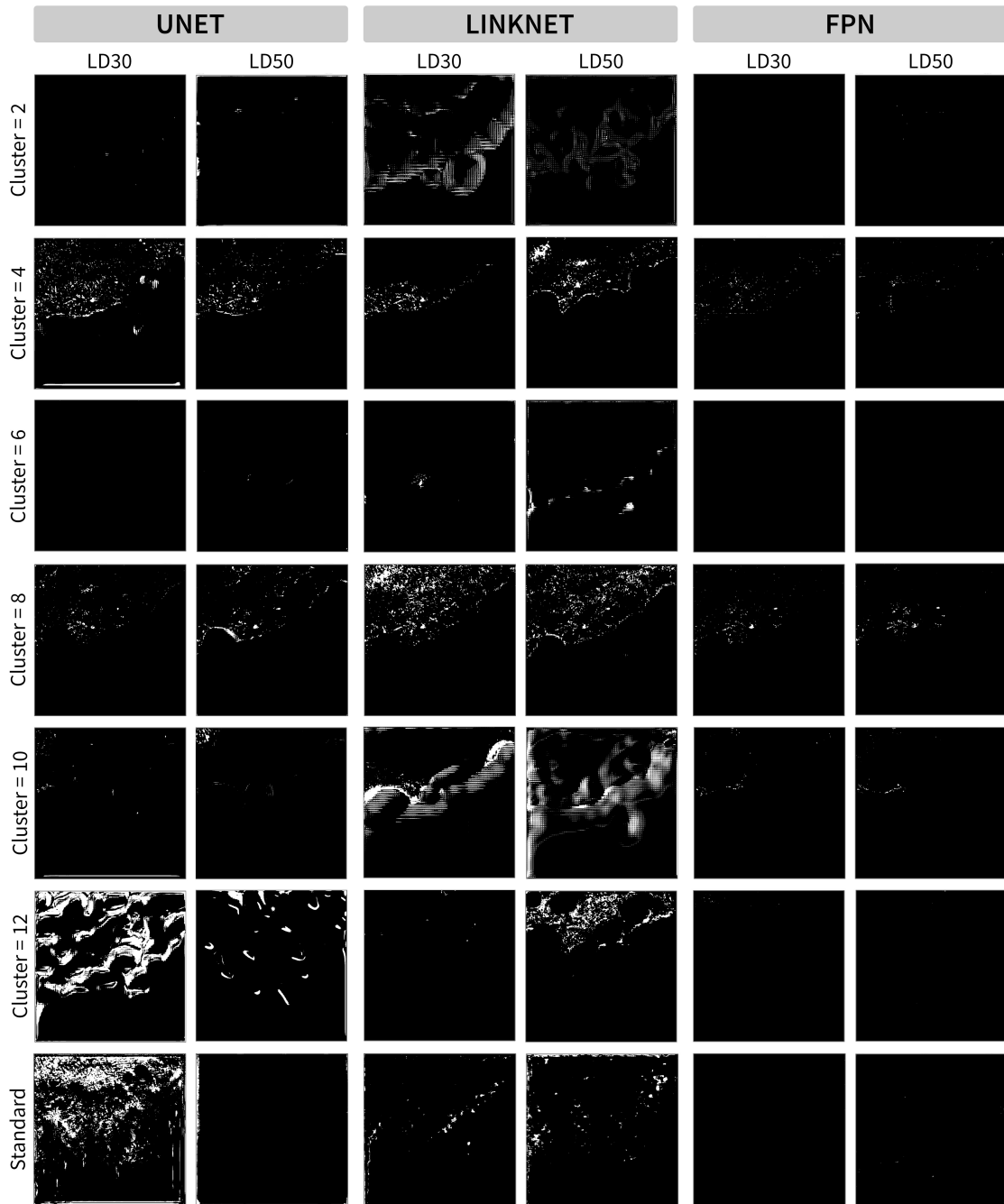


Figure 6: Predictions of landslides from the proposed and standard approaches.

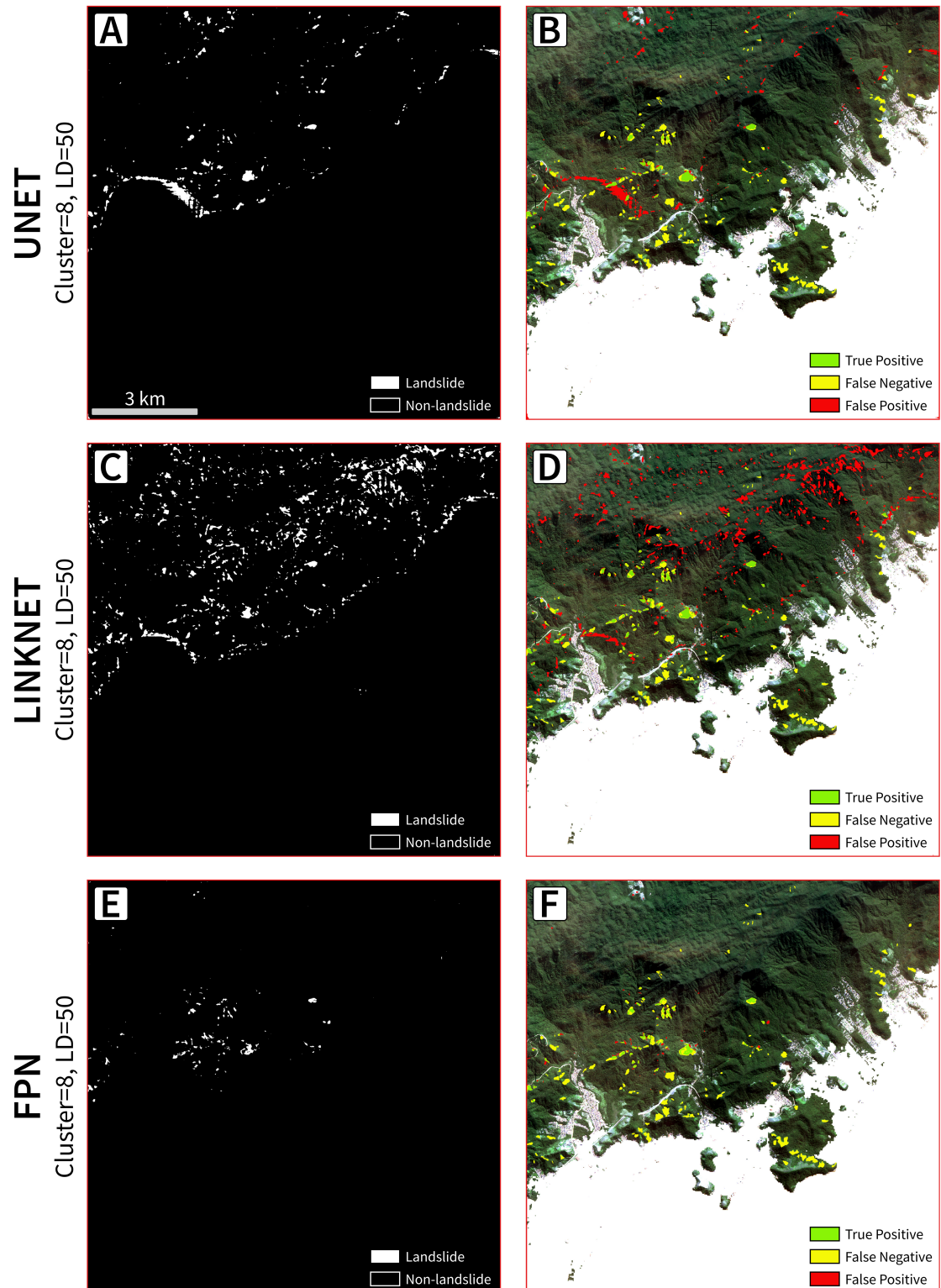


Figure 7: Image of True Positive, False Positive and False Negative samples from the predictions of (A) U-Net, (B) Linknet and (C) FPN. All predictions are from the combination of 8 clusters and LD50.

### Limitations on Relict Landslide Detection

Semi-automatic detection of relict landslides using CNNs in an area covered with vegetation proved to be a difficult task. CNNs successfully extract features from images, but satisfactory results rely mainly on the quality of input data and land cover characteristics. The results of validation indices and predictions demonstrate the difficulties in detecting relict landslides in vegetated areas. The high number of False Positives in these predictions is in accordance with the low precision values discussed earlier and is probably related to the input data used.

The main goal of this study is to detect relict landslides which are recognizable in this specific study area by the presence of *Gleichenella sp.* ferns that cover degraded areas, prevent forest restoration, and preserve the boundaries of landslides (Section 2.1.1). As shown in (Fig. 3, the relict landslides can be distinguished from surroundings by the light green color of *Gleichenella sp.* while native vegetation has a dark green color in general. However, there are spectral similarities between *Gleichenella sp.* ferns and other land cover features such as pasture, agricultural fields, or deforested areas. So the spectral characteristics are not enough to enable accurate detection of relict landslides, and the occurrence of misclassification is expected.

In areas covered by dense vegetation, such as the Atlantic rainforest, landslide detection is usually performed using multispectral images acquired soon after the event. In those images, landslides are easily recognizable due to the removal of material and soil exposure (Guzzetti et al., 1999; Du and Teng, 2007; Booth et al., 2009; Burns et al., 2010; Sameen and Pradhan, 2019). In multispectral images, the soil has a brown-orange color that contrasts with the surroundings' green color, making identification easier for the CNNs. Even in this case, errors and misclassifications are common (Soares et al., 2022).

Therefore there are limitations in semi-automatic detection of relict landslides in rainforest areas using multispectral images as input. These limitations are likely related to specificities of the input data like spatial and spectral resolution rather than the CNN semantic segmentation process itself.

For the best of the authors knowledge this is the first project to use CBERS-4A images for landslide detection. The mid to high spatial resolution (8 m) and 4 spectral bands (R, G, B and NIR) were insufficient to differentiate relict landslides from surroundings. Despite the adequate results of recall and the predictions that correctly identified relict landslides, the majority of the results were inaccurate. Spectral similarities prevented CNNs from achieving better results.

So, using high to very high spatial resolution images, or hyperspectral images, may overcome these limitations and achieve better and more accurate results for relict landslides detection. Also, using very high-resolution topographic data such as lidar that can be used to generate digital terrain models (DTM) by removing vegetation could enhance the accuracy of the semi-automatic detection of relict landslides.

### Discussion

This study found significant limitations in the semi-automatic detection of relict landslides in vegetation-covered areas using multispectral images as input to the CNN semantic segmentation process. These findings are essential to demonstrate that the accuracy of CNNs for landslide detection is closely related to the technical specificities of input data and the study area characteristics.

Also, a new CNN approach was proposed in an attempt to enhance landslide detection accuracy. The results demonstrate that the predictions of the proposed approach are better than those of the standard approach, but the values of precision and recall were very similar. The k means clustering

process used to create the Cluster dataset for the pre-training step that fine-tuned the CNN training process enhanced CNNs predictions ability. Another finding is that it was not possible to address an optimal correlation of parameters that maximizes the accuracy of landslide detection.

Most landslide detection studies are in areas with little to no vegetation cover and use post-event multispectral images when the landslides are clearly visible. Few studies occur in areas covered with rainforest vegetation (Sameen and Pradhan, 2019; Soares et al., 2022) or for detecting relict landslides (Wang et al., 2020). Also, many studies use a combination of topographic and spectral information as input for the CNNs (Ghorbanzadeh et al., 2019; Ji et al., 2020; Sameen and Pradhan, 2019; Wang et al., 2020).

Thus there is a lack of investigation in areas of tropical environments where landslides are common, and the monitoring is impaired by vegetation growth. The present study findings demonstrated the complexity of performing semi-automatic detection of relict landslides in rainforest areas and highlighted the importance of the input data specifications for the CNN models. It also showed the relevance of a continuous update of inventory maps.

This study has several specificities that prevent directly comparing the results with other works. However, many studies of landslide detection using CNNs also showed that both the input data and the study area are directly related to model accuracy (Chen et al., 2018; Ghorbanzadeh et al., 2019; Wang et al., 2020; Yu et al., 2021; Soares et al., 2022). The CBERS-4A images are the newer and best free data available for the mapping and monitoring of the Brazilian territory. Despite the great advance promoted in the area of remote sensing for Brazil, the CBERS-4A images were inappropriate for the detection of relict landslides in the specific conditions of this project. However they may yield better results if implemented with other conditions.

Although the results were generally inaccurate and the limitations of using multispectral images for relict landslide detection were exposed, the proposed approach proved to be a powerful tool for landslide detection. Even with all the limitations addressed previously, the CNN proposed approach could correctly predict relict landslides in almost half of the combinations (41.7%). Values of recall higher than 75% and the presence of False Positive samples do not represent a major concern once it is suitable for landslide detection studies to predict more landslides than in ground truth.

#### 4. Conclusion

This work proposed a new CNN approach for semi-automatic landslide detection, and the results were compared with a standard CNN approach. The proposed approach has a pre-training step that uses a dataset generated by a k-means algorithm clustering process as input. The weights computed in the pre-training step are later used to fine-tune the CNN training process. Two augmentation factors of 30 and 50 were used to increase the dataset, and three CNN (U-Net, Linknet and FPN) were used for semantic segmentation. Six combinations of CNN and parameters were generated for the standard approach and 36 for the proposed approach.

The recall was higher than 75% for every combination. The highest values were 79.53% for the standard approach combination of U-Net with LD30 and 80.95% for the proposed approach combination of U-Net with 10 clusters and LD50. In contrast, the precision values were very low for all combinations, generally between 10% and 20%. These low values are related to the high number of False Positives generated in the evaluation process.

Predictions of the landslide were performed in a test area to enhance the evaluation process for every combination of parameters. As a result, 15 of 42 combinations were able to identify landslide scars more or less accurately and with a high number of False Positives. Predictions

from the proposed approach were more accurate than those from the standard approach. Landslide scars located in the center-north portion of the test area were more easily detected than those in the center-south portion for the proposed approach. In contrast, for the standard approach, the landslide scars were identified in the whole area.

Overall, the proposed approach was better than the standard approach for landslide detection in the study area. The difference between recall and precision values was not so relevant, but the predictions of the proposed approach were more accurate. However, it was not possible to determine an optimal combination of parameters (type of CNN, number of clusters, augmentation factor) that best suit landslide detection or even a correlation between the parameters and the accuracy of the models. Predictions of all CNNs with clusters 4 and 8 yielded the best results. No CNN proved to be superior to the others.

Further investigation is needed to improve the proposed approach's accuracy, and the authors expect better results in areas with more visible landslides. Post-event images or usage of hyper-spectral imagery where landslides are better isolated from vegetation cover, with more spectral differences, may be used as input to test the proposed approach.

## Data Availability

CBERS images are available from INPE at <http://www2.dgi.inpe.br/catalogo/explore>. Python scripts and GIS vector data (landslide scars) are available at Github: [https://github.com/SPAMLab/data\\_sharing/tree/main/Relict\\_landslides\\_CNN\\_kmeans](https://github.com/SPAMLab/data_sharing/tree/main/Relict_landslides_CNN_kmeans).

## Funding details

This study was funded by the Sao Paulo Research Foundation (FAPESP) under grants #2016/06628-0, and #2019/26568-0; and Brazil's National Council of Scientific and Technological Development (CNPq) under grant #311209/2021-1. This study was financed in part by CAPES Brasil - Finance Code 001.

## Acknowledgements

The authors acknowledge the infrastructure and support of the Institute of Energy and Environment (IEE-USP) and the Graduate Program in Mineral Resources and Hydrogeology (RMH-IGc), Universidade de São Paulo, Brazil. This is a SPAMLab contribution (<https://spamlab.github.io/publications/>). Acknowledgements are extended to the Editor-in-Chief and the anonymous reviewers for their criticism and suggestions, which helped to improve this paper.

## ORCID

Guilherme Pereira Bento Garcia <https://orcid.org/0000-0003-1209-7842>  
Carlos Henrique Grohmann <https://orcid.org/0000-0001-5073-5572>  
Lucas Pedrosa Soares <https://orcid.org/0000-0002-6980-597X>  
Mateus Espadoto <https://orcid.org/0000-0002-1922-4309>

## References

### References

- Almeida, F. F. M., 1964. Fundamentos geológicos do relevo paulista. *Boletim do IGG* 41, 169–263.
- Ardizzone, F., Cardinali, M., Galli, M., Guzzetti, F., Reichenbach, P., 2007. Identification and mapping of recent rainfall-induced landslides using elevation data collected by airborne Lidar. *Natural Hazards and Earth System Science* 7 (6), 637–650.
- Audebert, N., Le Saux, B., Lefèvre, S., 2016. How useful is region-based classification of remote sensing images in a deep learning framework? *International Geoscience and Remote Sensing Symposium (IGARSS) 2016-November*, 5091–5094.
- Augusto Filho, O., 1992. Caracterização geológico-geotécnica voltada à estabilização de encostas: uma proposta metodológica. In: *conferência brasileira sobre estabilidade de encostas*. Vol. 1. pp. 721–733.
- Baldo, M., Bicocchi, C., Chiocchini, U., Giordan, D., Lollino, G., 2009. LIDAR monitoring of mass wasting processes: The Radicofani landslide, Province of Siena, Central Italy. *Geomorphology* 105 (3-4), 193–201.  
URL <http://dx.doi.org/10.1016/j.geomorph.2008.09.015>
- Booth, A. M., Roering, J. J., Perron, J. T., 2009. Automated landslide mapping using spectral analysis and high-resolution topographic data: Puget Sound lowlands, Washington, and Portland Hills, Oregon. *Geomorphology* 109 (3-4), 132–147.  
URL <http://dx.doi.org/10.1016/j.geomorph.2009.02.027>
- Brideau, M. A., Sturzenegger, M., Stead, D., Jaboyedoff, M., Lawrence, M., Roberts, N., Ward, B., Millard, T., Clague, J., 2012. Stability analysis of the 2007 Chehalis lake landslide based on long-range terrestrial photogrammetry and airborne LiDAR data. *Landslides* 9 (1), 75–91.
- Burns, W. J., Coe, J. A., Kaya, B. S., Ma, L., 2010. Analysis of elevation changes detected from multi-temporal LiDAR surveys in forested landslide terrain in western Oregon. *Environmental and Engineering Geoscience* 16 (4), 315–341.
- Burns, W. J., Madin, I. P., 2009. Protocol for Inventory Mapping of Landslide Deposits from Light Detection and Ranging (lidar) Imagery, 1–36.
- Casagli, N., Cigna, F., Bianchini, S., Hölbling, D., Füreder, P., Righini, G., Del Conte, S., Friedl, B., Schneiderbauer, S., Iasio, C., Vlcko, J., Greif, V., Prose, H., Granica, K., Falco, S., Lozzi, S., Mora, O., Arnaud, A., Novali, F., Bianchi, M., 2016. Landslide mapping and monitoring by using radar and optical remote sensing: Examples from the EC-FP7 project SAFER. *Remote Sensing Applications: Society and Environment* 4, 92–108.  
URL <http://dx.doi.org/10.1016/j.rsase.2016.07.001>
- Castelluccio, M., Poggi, G., Sansone, C., Verdoliva, L., 2015. Land Use Classification in Remote Sensing Images by Convolutional Neural Networks, 1–11.  
URL <http://arxiv.org/abs/1508.00092>
- Chaurasia, A., Culurciello, E., 2017. LinkNet: Exploiting encoder representations for efficient semantic segmentation. In: *IEEE Visual Communications and Image Processing (VCIP)*. p. 4.
- Chen, W., Li, X., Wang, Y., Chen, G., Liu, S., 2014. Forested landslide detection using LiDAR data and the random forest algorithm: A case study of the Three Gorges, China. *Remote Sensing of Environment* 152, 291–301.  
URL <http://dx.doi.org/10.1016/j.rse.2014.07.004>
- Chen, W., Li, X., Wang, Y., Liu, S., 2013. Landslide susceptibility mapping using LiDAR and DMC data: A case study in the Three Gorges area, China. *Environmental Earth Sciences* 70 (2), 673–685.
- Chen, Z., Zhang, Y., Ouyang, C., Zhang, F., Ma, J., 2018. Automated landslides detection for mountain cities using multi-temporal remote sensing imagery. *Sensors* 18 (821), 18.
- Cheng, G., Han, J., Lu, X., 2017. Remote sensing image scene classification: Benchmark and state of the art. *arXiv* 105 (10).
- Cheng, G., Yang, C., Yao, X., Guo, L., Han, J., 2018. When Deep Learning Meets Metric Learning: Remote Sensing Image Scene Classification via Learning Discriminative CNNs. *IEEE Transactions on Geoscience and Remote Sensing* 56 (5), 2811–2821.
- Conti, J. B., Furlan, S. A., 1996. *Geoecologia: o clima, os solos e a biota*. EDUSP.
- Correa, C. V. d. S., Reis, F. A. G. V., Giordano, L. C., Chaves, C. J., Gabelini, B. M., Cerri, R. I., 2017. Movimentos de massa na região de Caraguatatuba e São Sebastião (SP) entre 1967 e 2011: utilização de cicatrizes de escorregamento como subsídio a estudos de retro-análise. In: *XVII Simpósio Brasileiro de Geografia Física Aplicada/ I Congresso Nacional de Geografia Física*. Campinas, São Paulo, pp. 4162–4173.
- Derron, M. H., Jaboyedoff, M., 2010. LIDAR and DEM techniques for landslides monitoring and characterization. *Natural Hazards and Earth System Science* 10 (9), 1877–1879.

- Devoto, S., Macovaz, V., Mantovani, M., Soldati, M., Furlani, S., 2020. Advantages of using UAV digital photogrammetry in the study of slow-moving coastal landslides. *Remote Sensing* 12 (21), 3566–3594.
- Dias, H. C., Hölbling, D., Grohmann, C. H., 10 2021. Landslide susceptibility mapping in brazil: A review. *Geosciences* 11, 425.
- Ding, A., Zhang, Q., Zhou, X., Dai, B., 2016. Automatic recognition of landslide based on CNN and texture change detection. In: 31st Youth Academic Annual Conference of Chinese Association of Automation. Wuhan, China, pp. 444 – 448.
- Du, J. C., Teng, H. C., 2007. 3D laser scanning and GPS technology for landslide earthwork volume estimation. *Automation in Construction* 16 (5), 657–663.
- Ellenberg, H., Mueller Dombois, D., 1967. A key to raunkiaer plant life forms with revised subdivisions. *Ber. geobot. Inst. eidg. tech. Hochschule Rubel* 37, 56–73.
- Fukushima, K., 1980. Neocognitron: A self-organizing neural network model for a mechanism of pattern recognition unaffected by shift in position. *Biological Cybernetics* 36 (4), 193–202.
- Fúlfaro, V., Ponçano, W., Bistrichi, C., Stein, D., 1976. Escorregamentos de caraguatatuba: expressão atual, e registro na coluna sedimentar da planície costeira adjacente. In: Congresso brasileiro de geologia de engenharia. Vol. 2. pp. 341–350.
- Gariano, S. L., Guzzetti, F., 11 2016. Landslides in a changing climate. *Earth-Science Reviews* 162, 227–252.
- Ghorbanzadeh, O., Blaschke, T., Gholamnia, K., Meena, S. R., Tiede, D., Aryal, J., 2019. Evaluation of different machine learning methods and deep-learning convolutional neural networks for landslide detection. *Remote Sensing* 11 (196), 21.
- Ghuffar, S., Székely, B., Roncat, A., Pfeifer, N., 2013. Landslide displacement monitoring using 3D range flow on airborne and terrestrial LiDAR data. *Remote Sensing* 5 (6), 2720–2745.
- Glenn, N. F., Streutker, D. R., Chadwick, D. J., Thackray, G. D., Dorsch, S. J., 2006. Analysis of LiDAR-derived topographic information for characterizing and differentiating landslide morphology and activity. *Geomorphology* 73 (1-2), 131–148.
- Godone, D., Allasia, P., Borrelli, L., Gulla, G., 2020. UAV and structure from motion approach to monitor the Maierato landslide evolution. *Remote Sensing* 12 (6), 1039–1057.
- Guidicini, G., Nieble, C. M., 1984. Estabilidade de taludes naturais e de escavação. Editora Edgard Blücher. 2ª. Ed. São Paulo.
- Guzzetti, F., Carrara, A., Cardinali, M., Reichenbach, P., dec 1999. Landslide hazard evaluation: a review of current techniques and their application in a multi-scale study, Central Italy. *Geomorphology* 31 (1-4), 181–216.  
URL <https://www.sciencedirect.com/science/article/pii/S0169555X99000781?via%3Dihub>
- Guzzetti, F., Mondini, A. C., Cardinali, M., Fiorucci, F., Santangelo, M., Chang, K. T., 2012. Landslide inventory maps: New tools for an old problem. *Earth-Science Reviews* 112 (1-2), 42–66.  
URL <http://dx.doi.org/10.1016/j.earscirev.2012.02.001>
- He, K., Zhang, X., Ren, S., Sun, J., 2016. Deep residual learning for image recognition. pp. 770–778.
- Heleno, S., Matias, M., Pina, P., Sousa, A. J., apr 2016. Semiautomated object-based classification of rain-induced landslides with VHR multispectral images on Madeira Island. *Natural Hazards and Earth System Sciences* 16 (4), 1035–1048.  
URL <https://www.nat-hazards-earth-syst-sci.net/16/1035/2016/>
- Huang, G., Liu, Z., Maaten, L. V. D., Weinberger, K. Q., jul 2017. Densely connected convolutional networks. In: 2017 IEEE Conference on Computer Vision and Pattern Recognition (CVPR). IEEE Computer Society, Los Alamitos, CA, USA, pp. 2261–2269.  
URL <https://doi.ieeecomputersociety.org/10.1109/CVPR.2017.243>
- Iwahashi, J., Kamiya, I., Yamagishi, H., 2012. High-resolution DEMs in the study of rainfall- and earthquake-induced landslides: Use of a variable window size method in digital terrain analysis. *Geomorphology* 153-154, 29–38.  
URL <http://dx.doi.org/10.1016/j.geomorph.2012.02.002>
- Jaboyedoff, M., Oppikofer, T., Abellán, A., Derron, M. H., Loye, A., Metzger, R., Pedrazzini, A., 2012. Use of LIDAR in landslide investigations: A review. *Natural Hazards* 61 (1), 5–28.
- Jebur, M. N., Pradhan, B., Tehrany, M. S., 2014. Optimization of landslide conditioning factors using very high-resolution airborne laser scanning (LiDAR) data at catchment scale. *Remote Sensing of Environment* 152, 150–165.  
URL <http://dx.doi.org/10.1016/j.rse.2014.05.013>
- Ji, S., Yu, D., Shen, C., Xu, Q., 2020. Landslide detection from an open satellite imagery and digital elevation model dataset using attention boosted convolutional neural networks. *Landslides* 17, 1337 – 1352.
- Jia, Y., Shelhamer, E., Donahue, J., Karayev, S., Long, J., Girshick, R., Guadarrama, S., Darrell, T., 11 2014. Caffe. *ACM*, pp. 675–678.

- Kasai, M., Ikeda, M., Asahina, T., Fujisawa, K., 2009. LiDAR-derived DEM evaluation of deep-seated landslides in a steep and rocky region of Japan. *Geomorphology* 113 (1-2), 57–69.  
URL <http://dx.doi.org/10.1016/j.geomorph.2009.06.004>
- Kawabata, D., Bandibas, J., 2009. Landslide susceptibility mapping using geological data, a DEM from ASTER images and an Artificial Neural Network (ANN). *Geomorphology* 113 (1-2), 97–109.  
URL <http://dx.doi.org/10.1016/j.geomorph.2009.06.006>
- Knevels, R., Petschko, H., Leopold, P., Brenning, A., 2019. Geographic Object-Based Image Analysis for Automated Landslide Detection Using Open Source GIS Software. *International Journal of Geo-Information* 8 (551), 21.
- Koeppen, W., 1948. *Climatologia: con un estudio de los climas de la tierra*, 478 p.
- Krizhevsky, A., Sutskever, I., Hinton, G. E., 2012. ImageNet Classification with Deep Convolutional Neural Networks. In: *Conf. Adv. Neural Inf. Process.* pp. 1097–1105.
- Kronka, J., et al., 2007. Inventário florestal da vegetação natural do estado de são paulo. regiões administrativas de são jose dos campos (litoral), baixada santista e registro.
- Kussul, N., Lavreniuk, M., Skakun, S., Shelestov, A., 2017. Deep Learning Classification of Land Cover and Crop Types Using Remote Sensing Data. *IEEE Geoscience and Remote Sensing Letters* 14 (5), 778–782.
- LeCun, Y., Boser, B., Denker, J. S., Henderson, D., Howard, R. E., Hubard, W., Jackel, D., 1989. Backpropagation applied to handwritten zip code recognition. *Neural Computation* 1 (4), 541–551.
- Lehmann, D., 2008. Estudos Sobre a Propagação De *Gleichenella Pectinata* (Willd.) Ching (Pteridófitas - Gleicheniaceae). Dissertação de mestrado.
- Li, C., Yi, B., Gao, P., Li, H., Sun, J., Chen, X., Zhong, C., 2021. Valuable clues for DCNN-Based landslide detection from a comparative assessment in the Wenchuan earthquake area. *Sensors* 21 (5191), 14.
- Li, S., Xiong, L., Tang, G., Strobl, J., 2020. Deep learning-based approach for landform classification from integrated data sources of digital elevation model and imagery. *Geomorphology* 354, 1–14.
- Li, X., Cheng, X., Chen, W., Chen, G., Liu, S., 2015. Identification of forested landslides using lidar data, object-based image analysis, and machine learning algorithms. *Remote Sensing* 7 (8), 9705–9726.
- Lin, C.-W., Tseng, C.-M., Tseng, Y.-H., Fei, L.-Y., Hsieh, Y.-C., Tarolli, P., jan 2013. Recognition of large scale deep-seated landslides in forest areas of Taiwan using high resolution topography. *Journal of Asian Earth Sciences* 62, 389–400.  
URL <https://linkinghub.elsevier.com/retrieve/pii/S136791201200452X>
- Lin, T.-Y., Dollar, P., Girshick, R., He, K., Hariharan, B., Belongie, S., 2017. Feature Pyramid Networks for Object Detection. In: *IEEE Conference on Computer Vision and Pattern Recognition (CVPR)*. pp. 2117 – 2125.
- Lindner, G., Schraml, K., Mansberger, R., Hubl, J., 2016. UAV monitoring and documentation of a large landslide. *Applied Geomatics* 8, 1–11.
- Lingua, a., Piatti, D., Rinaudo, F., 2008. Remote monitoring of landslide using an integration of GB-INSAR and Lidar techniques. *The internal archives of the photogrammetry, remote sensing and spatial information sciences*, Volume XXXVII, 361–366.
- Liu, J.-K., Chang, K.-T., Rau, J.-Y., Hsu, W.-C., Liao, Z.-Y., Lau, C.-C., Shih, T.-Y., 2009. The geomorphometry of rainfall-induced landslides in taiwan obtained by airborne lidar and digital photography. In: *Geoscience and Remote Sensing. InTech*.
- Lucier, A., de Jong, S. M., Turner, D., 2014. Mapping landslide displacements using Structure from Motion (SfM) and image correlation of multi-temporal UAV photography. *Progress in Physical Geography* 38 (1), 97–116.
- Luus, F. P. S., Salmon, B. P., van den Bergh, F., Maharaj, B. T. J., 2015. Multiview Deep Learning for Land-Use Classification. *IEEE GEOSCIENCE AND REMOTE SENSING LETTERS* 12 (12), 2448–2452.
- Ma, L., Liu, Y., Zhang, X., Ye, Y., Yin, G., Johnson, B. A., 2019. Deep learning in remote sensing applications: A meta-analysis and review. *ISPRS Journal of Photogrammetry and Remote Sensing* 152 (November 2018), 166–177.  
URL <https://doi.org/10.1016/j.isprsjprs.2019.04.015>
- Mantovani, F., Soeters, R., VAN Westen, C. J., 1996. Remote sensing techniques for landslide studies and hazard zonation in Europe. *Geomorphology* 15, 213–225.  
URL [https://ac.els-cdn.com/0169555X9500071C/1-s2.0-0169555X9500071C-main.pdf?{}\\_tid=e636cc36-64b3-45b5-9b18-41c5724cc837{&}acdnat=1547762487{ }51f2ebff6e0f6d1e2568d0e647e7d2e1](https://ac.els-cdn.com/0169555X9500071C/1-s2.0-0169555X9500071C-main.pdf?{}_tid=e636cc36-64b3-45b5-9b18-41c5724cc837{&}acdnat=1547762487{ }51f2ebff6e0f6d1e2568d0e647e7d2e1)
- Marcelino, E. V., 2004. Mapeamento de áreas susceptíveis a escorregamento no município de Caraguatatuba (SP) usando técnicas de Sensoriamento Remoto. Dissertação de mestrado.
- Maxwell, A. E., Warner, T. A., Fang, F., 2018. Implementation of machine-learning classification in remote sensing: an applied review. *International Journal of Remote Sensing* 39 (9), 2784–2817.
- McKean, J., Roering, J., 2004. Objective landslide detection and surface morphology mapping using high-resolution airborne laser altimetry. *Geomorphology* 57 (3-4), 331–351.

- Menegoni, N., Giordan, D., Perotti, C., 2020. Reliability and uncertainties of the analysis of an unstable rock slope performed on RPAS digital outcrop models: The case of the Gallivaggio landslide (Western Alps, Italy). *Remote Sensing* 12 (10), 1635–1660.
- Metternicht, G., Hurni, L., Gogu, R., 2005. Remote sensing of landslides: An analysis of the potential contribution to geo-spatial systems for hazard assessment in mountainous environments. *Remote Sensing of Environment* 98 (2-3), 284–303.
- Mozas-Calvache, A. T., Pérez-garcía, J. L., Fernandez-del Castillo, T., 2017. Monitoring of landslides displacements using UAS and control methods based on lines. *Landslides* 14, 2115–2128.
- Netto, A. L. C., Sato, A. M., Avelar, A. S., Vianna, L. G. G., Araújo, I. S., Ferreira, D. L. C., Lima, P. H., Silva, A. P. A., Silva, R. P., 2011. January 2011: the extreme landslide disaster in Brazil. In: *Proceedings of the 2nd World Landslide Forum*. p. 6.
- Niethammer, U., Rothmund, S., James, M. R., Travelletti, J., Joswig, M., 2010. UAV-Based Remote Sensing of Landslides. In: *International Archives of Photogrammetry, Remote Sensing and Spatial Information Sciences*. pp. 496–501.
- Nilsen, T. H., Brabb, E. E., 1973. Current slope stability studies in the San Francisco bay region. *Journal Research U.S. Geological Survey* 1 (4), 431–437.
- Nohani, E., Moharrami, M., Sharafi, S., Khosravi, K., Pradhan, B., Pham, B. T., Lee, S., Melesse, A. M., 2019. Landslide Susceptibility Mapping Using Different GIS-Based Bivariate Models. *Water* 11 (1402), 1–22.
- Pal, M., Mather, M., 2006. Support vector machines for classification in remote sensing. *International Journal of Remote Sensing* 26 (5), 1007–1011.
- Pedregosa, F., Varoquaux, G., Gramfort, A., Michel, V., Thirion, B., Grisel, O., Blondel, M., Prettenhofer, P., Weiss, R., Dubourg, V., Vanderplas, J., Passos, A., Cournapeau, D., Brucher, M., Perrot, M., Duchesnay, E., 2011. Scikit-learn: Machine learning in Python. *Journal of Machine Learning Research* 12, 2825–2830.
- Perrota, M. M., Salvador, E. D., Lopes, R. C., D’Agostino, L. Z., Peruffo, N., Gomes, S. D., Sachs, L. L. B., Meira, V. T., Garcia, M. G. M., Lacerda Filho, J. V., 2005. Mapa Geológico do Estado de São Paulo. Tech. rep., CPRM, São Paulo, Brasil.
- Petropoulos, G. P., Kalaitzidis, C., Prasad Vadrevu, K., 2012. Support vector machines and object-based classification for obtaining land-use/cover cartography from Hyperion hyperspectral imagery. *Computers and Geosciences* 41, 99–107.  
URL <http://dx.doi.org/10.1016/j.cageo.2011.08.019>
- Ponçano, W. L., 1981. Mapa geomorfológico do estado de São Paulo. Vol. 1. Instituto de Pesquisas Tecnológicas do Estado de São Paulo, Divisão de Minas . . . .
- Portela, V. D. A., 2014. Avaliação da vegetação como indicadora de áreas suscetíveis a escorregamentos na Serra do Mar em Caraguatatuba (SP). áreas suscetíveis a escorregamentos na Serra do Mar em Caraguatatuba ( SP ) Viviane Dias Alves Portela Avaliação da vegetação como indicad. Dissertação de mestrado.
- Prakash, N., Manconi, A., Loew, S., 2020. Mapping Landslides on EO Data: Performance of Deep Learning vs. Traditional Machine Learning Models. *Remote Sensing* 12 (346), 24.
- Roering, J. J., Kirchner, J. W., Dietrich, W. E., 2005. Characterizing structural and lithologic controls on deep-seated landsliding : Implications for topographic relief and landscape evolution in the Oregon Coast Range , USA (5), 654–668.
- Roering, J. J., Mackey, B. H., Marshall, J. A., Sweeney, K. E., Deligne, N. I., Booth, A. M., Handwerker, A. L., Cerovski-Darriau, C., oct 2013. ‘You are HERE’: Connecting the dots with airborne lidar for geomorphic fieldwork. *Geomorphology* 200, 172–183.  
URL <https://linkinghub.elsevier.com/retrieve/pii/S0169555X13002031>
- Ronneberger, O., Fischer, P., Brox, T., 2015. U-Net: Convolutional Networks for Biomedical Image Segmentation. In: *Medical Image Computing and Computer-Assisted Intervention*. pp. 234–241.
- Sameen, M. I., Pradhan, B., 2019. Landslide detection using residual networks and the fusion of spectral and topographic information. *IEEE Access* 7, 114363 – 114373.
- Samodra, G., Ramadhan, M. F., Sartohadi, J., Setiawan, M. A., Christanto, N., Sukmawijaya, A., 2020. Characterization of displacement and internal structure of landslides from multitemporal UAV and ERT imaging. *Landslides* 17, 2455–2468.
- Scaioni, M., Longoni, L., Melillo, V., Papini, M., 2014. Remote Sensing for Landslide Investigations: An Overview of Recent Achievements and Perspectives. *Remote Sensing* 6, 53.
- Schulz, W. H., 2007. Landslide susceptibility revealed by LIDAR imagery and historical records, Seattle, Washington. *Engineering Geology* 89 (1-2), 67–87.
- Scott, G. J., England, M. R., Starns, W. A., Marcum, R. A., Davis, C. H., 2017. Training Deep Convolutional

- Neural Networks for Land-Cover Classification of High-Resolution Imagery. *IEEE Geoscience and remote sensing letters* 14 (4), 549–553.
- Shahabi, H., Hashim, M., 2015. Landslide susceptibility mapping using GIS-based statistical models and remote sensing data in tropical environment. *Scientific Reports* 5 (9899), 15.
- Simonyan, K., Zisserman, A., 2014. Very deep convolutional networks for large-scale image recognition.
- Soares, L. P., Dias, H. C., Garcia, G. P. B., Grohmann, C. H., 2022. Landslide segmentation with deep learning: Evaluating model generalization in rainfall-induced landslides in Brazil. *Remote Sensing* 14, 2237.
- Summerfield, M. A., 1991. *Global Geomorphology*, 1st Edition. Pearson Education Limited, Edinburgh.
- Szegedy, C., Liu, W., Jia, Y., Sermanet, P., Reed, S., Anguelov, D., Erhan, D., Vanhoucke, V., Rabinovich, A., 2015. Going deeper with convolutions. pp. 1–9.
- Tominaga, L. K., Santoro, J., do Amaral, R., 2009. *Desastres naturais: conhecer para prevenir*. Instituto geológico.
- Turner, D., Lucieer, A., de Jong, S. M., 2015. Time series analysis of landslide dynamics using an Unmanned Aerial Vehicle (UAV). *Remote Sensing* 7, 1736–1757.
- UNISDR, 2015. Sendai framework for disaster risk reduction 2015-2030. Tech. rep., The United Nations Office for Disaster Risk Reduction, Geneva, Switzerland.
- Van Den Eeckhaut, M., Kerle, N., Poesen, J., Hervás, J., 2012. Object-oriented identification of forested landslides with derivatives of single pulse LiDAR data. *Geomorphology* 173-174, 30–42.  
URL <http://dx.doi.org/10.1016/j.geomorph.2012.05.024>
- Van Den Eeckhaut, M., Poesen, J., Gullentops, F., Vandekerckhove, L., Hervás, J., 2011. Regional mapping and characterisation of old landslides in hilly regions using LiDAR-based imagery in Southern Flanders. *Quaternary Research* 75 (3), 721–733.  
URL <http://dx.doi.org/10.1016/j.yqres.2011.02.006>
- Van Den Eeckhaut, M., Poesen, J., Verstraeten, G., Vanacker, V., Moeyersons, J., Nyssen, J., van Beek, L. P. H., 2005. The effectiveness of hillshade maps and expert knowledge in mapping old deep-seated landslides. *Geomorphology* 67 (3-4), 351–363.
- Van Den Eeckhaut, M., Poesen, J., Verstraeten, G., Vanacker, V., Nyssen, J., Moeyersons, J., van Beek, L. P. H., Vandekerckhove, L., 2007. Use of LIDAR-derived images for mapping old landslides under forest. *Earth Surface Processes and Landforms* 32 (September), 754–769.  
URL <http://doi.wiley.com/10.1002/esp.1730>
- van Westen, C. J., Castellanos, E., Kuriakose, S. L., 2008. Spatial data for landslide susceptibility, hazard, and vulnerability assessment: An overview. *Engineering Geology* 102 (3-4), 112–131.  
URL <http://dx.doi.org/10.1016/j.enggeo.2008.03.010>
- Veloso, H. P., Rangel-Filho, A. L. R., Lima, J. C. A., 1991. *Classificação da vegetação brasileira, adaptada a um sistema universal*. IBGE.
- Ventura, G., Vilardo, G., Terranova, C., Sessa, E. B., 2011. Tracking and evolution of complex active landslides by multi-temporal airborne LiDAR data: The Montaguto landslide (Southern Italy). *Remote Sensing of Environment* 115 (12), 3237–3248.  
URL <http://dx.doi.org/10.1016/j.rse.2011.07.007>
- Wang, G., Joyce, J., Phillips, D., Shrestha, R., Carter, W., 2013. Delineating and defining the boundaries of an active landslide in the rainforest of Puerto Rico using a combination of airborne and terrestrial LIDAR data. *Landslides* 10 (4), 503–513.
- Wang, H., Zhang, L., Yin, K., Luo, H., Li, J., 2020. Landslide identification using machine learning. *Geoscience Frontiers*, 1–14.
- Werbos, P., 1974. *Beyond Regression: New tools for prediction and analysis in the behavioral science*. Ph.D. thesis, Harvard University.
- Wolle, C. M., 1988. *Análise de escorregamentos translacionais numa região da Serra do Mar no contexto de uma classificação de mecanismos de instabilização de encostas*. Tese de doutorado, Universidade de São Paulo.
- Xu, Q., Li, W.-l., Ju, Y.-z., Dong, X.-j., Peng, D.-l., 2020. Multitemporal UAV-based photogrammetry for landslide detection and monitoring in a large area: a case study in the Heifangtai terrace in the Loess Plateau of China. *Journal of Mountain Science* 14, 1826–1839.
- Yakovovskiy, P., 2019. Segmentation models. [https://github.com/qubvel/segmentation\\_models](https://github.com/qubvel/segmentation_models).
- Yu, B., Chen, F., Xu, C., Wang, L., Wang, N., 2021. Matrix SegNet: A practical deep learning framework for landslide mapping from images of different areas with different spatial resolutions. *Remote Sensing* 13 (3158), 16.
- Yu, M., Huang, Y., Zhou, J., Mao, L., 2017. Modeling of landslide topography based on micro-unmanned aerial vehicle photography and structure-from-motion. *Environmental Earth Sciences* 76 (520), 9.
- Zhang, L., Zhang, L., Kumar, V., 2016. Deep learning for Remote Sensing Data. *IEEE Geoscience and Remote*

- Sensing Magazine 4 (2), 22–40.
- Zhao, W., Du, S., Emery, W. J., 2017. Object-Based Convolutional Neural Network for High-Resolution Imagery Classification. *IEEE Journal of Selected Topics in Applied Earth Observations and Remote Sensing* 10 (7), 3386–3396.
- Zhao, W., Guo, Z., Yue, J., Zhang, X., Luo, L., 2015. On combining multiscale deep learning features for the classification of hyperspectral remote sensing imagery. *International Journal of Remote Sensing* 36 (13), 3368–3379.  
URL <http://dx.doi.org/10.1080/2150704X.2015.1062157>
- Zhong, L., Hu, L., Zhou, H., 2019. Deep learning based multi-temporal crop classification. *Remote Sensing of Environment* 221 (November 2018), 430–443.  
URL <https://doi.org/10.1016/j.rse.2018.11.032>
- Zhong, Y., Fei, F., Liu, Y., Zhao, B., Jiao, H., Zhang, L., 2017. SatCNN: satellite image dataset classification using agile convolutional neural networks. *Remote Sensing Letters* 8 (2), 136–145.  
URL <http://dx.doi.org/10.1080/2150704X.2016.1235299>